IEEE Photonics Journal
An IEEE Photonics Society Publication

High Energy Ultrafast Laser at 2 μm Using Dispersion Engineered Thulium-Doped Fiber

(Invited Paper)

Volume 11, Number 6, December 2019

Yuhao Chen
Shaoxiang Chen
Raghuraman Sidharthan
Chen Jian Cheng
Kun Liu
Shreesha Rao D. S.
Ole Bang
Qijie Wang
DingYuan Tang
Seongwoo Yoo

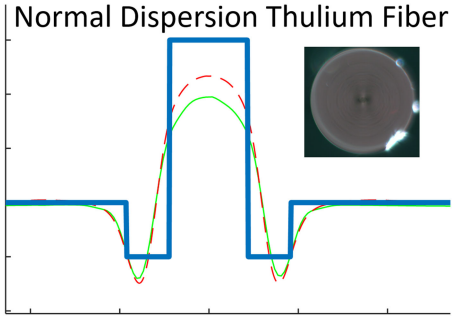

DOI: 10.1109/JPHOT.2019.2945928

High Energy Ultrafast Laser at 2 μm Using Dispersion Engineered Thulium-Doped Fiber

(Invited Paper)

Yuhao Chen,[1] Shaoxiang Chen,[1] Raghuraman Sidharthan,[1] Chen Jian Cheng,[1] Kun Liu,[1] Shreesha Rao D. S.,[2] Ole Bang,[2] Qijie Wang,[1] DingYuan Tang,[1] and Seongwoo Yoo[1]

[1]School of Electrical and Electronic Engineering, Nanyang Technological University, Singapore 639798
[1]DTU Fotonik, Department of Photonics Engineering, Technical University of Denmark, Kongens Lyngby 2800, Denmark

DOI:10.1109/JPHOT.2019.2945928

Manuscript received July 31, 2019; revised September 16, 2019; accepted October 1, 2019. Date of publication October 7, 2019; date of current version November 5, 2019. This work was supported in part by Academic Research Fund Tier 1, Ministry of Education (Singapore) under Project Grant 2018-T1-001-148 (RG 84/18), in part by Horizon 2020 Framework Programme (H2020) Research and Innovation Program under Marie Skłodowska-Curie (722380) (SUPUVIR), and in part by EDB IPP project under Grant S16-1257-IPP COY-15-IPP/160006 in association with Sintec Optronics Pte. Ltd. Corresponding author: Yuhao Chen (e-mail: ychen055@e.ntu.edu.sg).

Abstract: We report on demonstration of high energy pulse laser at 2 μm by employing a normal dispersion fiber attained by a waveguide dispersion engineering. The normal dispersion fiber has a W-type refractive index profile, with a Thulium(Tm)-doped core. In contrast to a strong anomalous dispersion at 2 μm in a step-index fiber, the design allows strong waveguide dispersion that can generate normal dispersion at the Tm emission band. Mode area scalability of this fiber is discussed under the normal dispersion requirement. The Tm-doped fiber (TDF) is deployed in a ring cavity to produce mode-locked pulses near 2 μm. Subsequently, the pulse is amplified with more than 27 dB gain through the normal dispersion TDF. The output pulse energy reaches up to $\sim$525 nJ at 1852 nm without pulse breaking due to the engineered dispersion. The achieved pulse energy is record high for all-fiber configuration near 2 μm, to our knowledge.

Index Terms: Specialty fiber, fiber lasers, Thulium, ultrashort pulses, dispersion shift.

1. Introduction

A 2 μm laser offers a myriad of unique material processing applications compared to the conventional 1 μm wavelength. Firstly, most semiconductors are transparent at 2 μm wavelength, which allows laser to focus to specific target layers for micro machining [1]. Secondly, plastic processing would be more efficient as it has much higher absorption at 2 μm [2]. Thirdly, biological tissue processing would also see benefits due to the water absorption peak near to 2 μm wavelength [3]. On the other hand, high energy ultrashort pulses enables precision micromachining by impacting high energy over time periods shorter than the material response time. The ultrafast laser reduces a heat affected zone, thus vastly increasing the quality of micromachining [4]. Hence, the confluence of these advantages, 2 μm high energy ultrashort pulses have the potential to bring precision

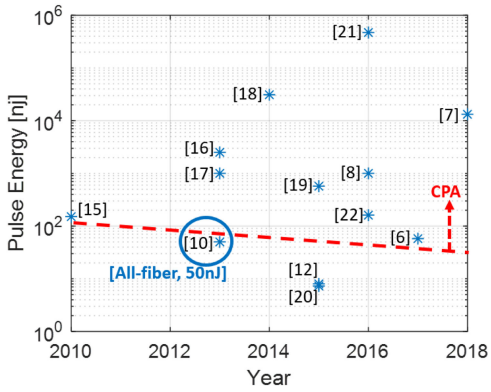

Fig. 1. Recent progress of ultrafast pulse energy at 2 μm. CPA: Chirped Pulse Amplification. The pulse energies above the red broken line were achieved via CPA. The blue circled result used normal dispersion Tm-doped fiber.

processing and micromachining applications to other exotic non-metallic materials which is beyond what 1 μm pulsed laser can offer.

Conventional ultrafast fiber laser at 2 μm relies on Thulium(Tm)-Doped-Fibers (TDFs) whose dispersion is conventionally anomalous at 2 μm. With the anomalous dispersion, pulse energy scaling is fundamentally limited due to soliton fission, defined by the soliton area theorem [5]. This limitation has hindered progress of 2 μm ultrafast fiber laser. To avoid the pulse breaking-up, chirp pulse amplification (CPAs) has to be employed to obtain power above the limited soliton energy. Fig. 1 summarizes the recent progress of ultrafast pulse energy at 2 μm. Clearly, the chart suggests pulse energy scaling above 100 nJ requires CPA. Specialty fibers such as Tm:ZBLAN [6], Tm:PCF fiber [7], or large mode area (LMA)-TDF [8], [9] have been often utilized for high energy demonstration with free space coupling. On the other hand, the maximum pulse energy achieved from all-fiber system stays around 50 nJ [10]. Further energy scaling should rely on multiple stages of CPA, depending on required energy, which extremely complicates architecture. Alternatively, it is possible to maintain a net cavity dispersion as normal dispersion to increase the pulse energy [11], [12]. The net normal dispersion cavity relies on introducing very long normal dispersion passive fiber, e.g., ultra-high-NA (UHNA) fiber, to compensate the anomalous dispersion from Tm fiber [13]. However, optical gain is still generated through the anomalous TDF, the net normal dispersion does not completely remove pulse breaking [14].

To respond to this problem, there was also an attempt to develop a normal dispersion Tm fiber by changing the material dispersion in [20], but the resultant pulse energy was low. Thus, it is obvious to have an efficient normal dispersion TDF for the interest of pulse energy scaling in a compact and robust all-fiber architecture. Here, we report a design and fabrication of a Normal Dispersion Tm-doped Fiber (NDTF) with a W-type refractive index profile (RIP) which unlike micro-structured fiber can enjoy a full access to fiber components made of a Single-Mode Fiber (SMF) to build a fiberized system. A mode-locked laser is achieved using a saturable absorber. Further, we built an all-fiber amplifier using the NDTF to extract pulse energy of $\sim$525 nJ without pulse breaking. To our knowledge, this is the highest pulse energy from an all-fiber architecture at the 2 μm region, as compared to previous reports of $<$4 nJ pulse using a normal dispersion TDF [20], and 50 nJ pulse energy using a commercial anomalous Tm fiber [10].

2. Fiber Design and Fabrication

2.1 Refractive Index Profile (RIP) Design

Fiber dispersion is determined by material dispersion and waveguide dispersion. While it is very limited to adjust the material dispersion in a silica fiber, the waveguide dispersion is considerably

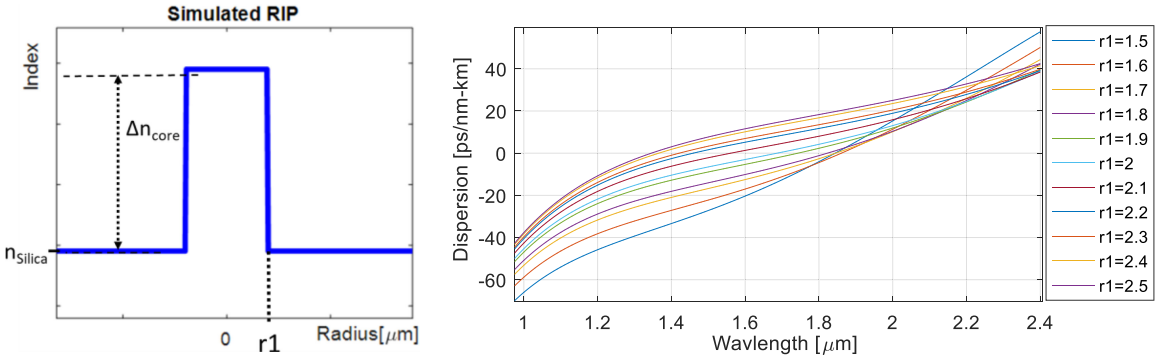

a) b)

Fig. 2. (a) A step-index fiber refractive index profile (RIP) indicating the variables of core index difference, Δn_{core}, with respect to the refractive index of silica cladding, n_{silica}, and core radius, *r1*. (b) Spectral response of dispersion with *r1*.

engineerable by modifying fiber parameters such as a core size, a core NA [23] or micro-structuring [24], which enhances the interaction of an evanescent field of a guided mode with cladding [23]. We first explore a simple step-index design to achieve the desired dispersion property at 2 μm. Fig. 2(a) represents the step-index profile with two important parameters of a core index difference, Δn_{core}, and a core radius, *r1*. To have a reasonable pump absorption, a certain amount of Tm concentration is necessary in the core together with sufficient Aluminum (Al) to avoid concentration quenching [25]. In a conventional modified chemical vapor deposition (MCVD) process, $\sim$7 mol% of Al_2O_3 is achievable through a solution doping technique. Such amount of Al_2O_3 concentration raises refractive index to 0.015 [26]. Hence, we set Δn_{core} at 0.015 and adjust *r1* to study contribution of waveguide dispersion. A silica glass refractive index is assumed for the cladding index, factoring in its material dispersion through Sellmeier's formula [27].

The influence of *r1* on the fiber dispersion is represented in Fig. 2(b). With decreasing *r1* from 2.5 μm to 1.5 μm, the Zero Dispersion Wavelength (ZDW) is shifted to longer wavelengths. However, when *r1* reaches 1.8 μm and below, the slope at the longer wavelength steeply increases, indicating leaking of a guided mode. For example, at $r1 = 1.5$ μm (the blue curve), the guided mode becomes leaky just after the wavelength of 1.6 μm. Hence, a core radius of 1.5 μm is too small for guiding light at 2 μm. It seems the core radius of 2.1 μm is suitable for the desired 2 μm operation but with anomalous dispersion. Hence, this study illustrates the limitation of a normal step index fiber for dispersion control. To enhance waveguide dispersion, a trench cladding [28] such as a W-shaped index profile can be used, as represented in Fig. 3(a). As before, the core index difference, Δn_{core}, is set at 0.015. In addition, we fix the Δn_{trench} at -0.005, which is practical for the MCVD process with Fluorine (F) dopant. Its corresponding concentration is $\sim$ 1 mol% if all doped F is assumed to form SiF_4.

As shown in Fig. 3(b), with a fixed *r1* at 2.2 μm, *r2* is varied to adjust a dispersion property. The trench introduces a dip in the dispersion curve due to waveguide dispersion, which enhances normal dispersion at the 2 μm region. The position of the dip in the dispersion curve is indicated in Fig. 3(b). As *r2* increases, the dip becomes more pronounced. For example, at $r2 = 5$ μm (the purple curve), the dip goes just below -50 ps/nm-km. And at $r2 = 6$ μm (the teal curve), the dip goes below -100 ps/nm-km. However, a larger dip creates steeper slope at the longer wavelength edge, which indicates leakage. It is concluded that with the set index differences and the core radius, the *r2* of 4.6 μm would offer the best compromise for normal dispersion and robust guidance in this design setting.

With the determined *r2*, we attempt to scale the core size, *r1*, to increase storable energy. Fig. 4(a) represents dispersion response to the increasing core size. As expected, the increasing core size reduces the dip in the dispersion curve as it strengthens guidance and reduces evanescent field

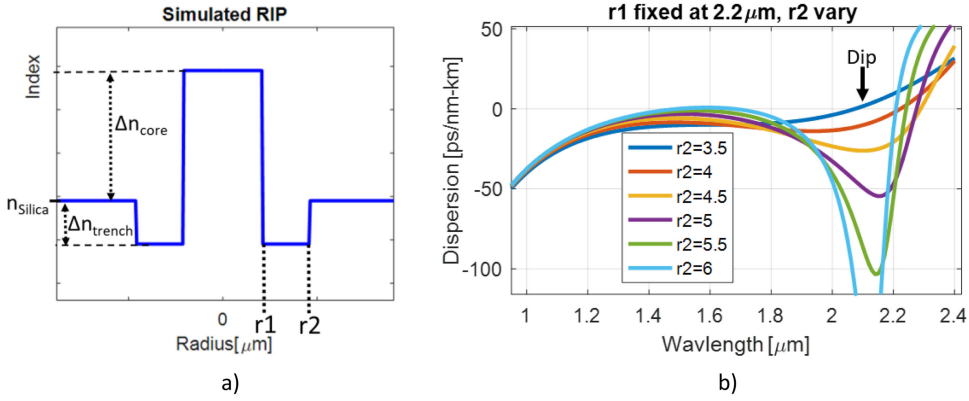

Fig. 3. (a) A W-type fiber RIP indicating the variables of core index difference, Δn_{core}, trench index difference, Δn_{trench}, with respect to the refractive index of silica cladding, n_{silica}, core radius, *r1*, and trench radius, *r2*. (b) Spectral response of dispersion to trench radius, *r2*.

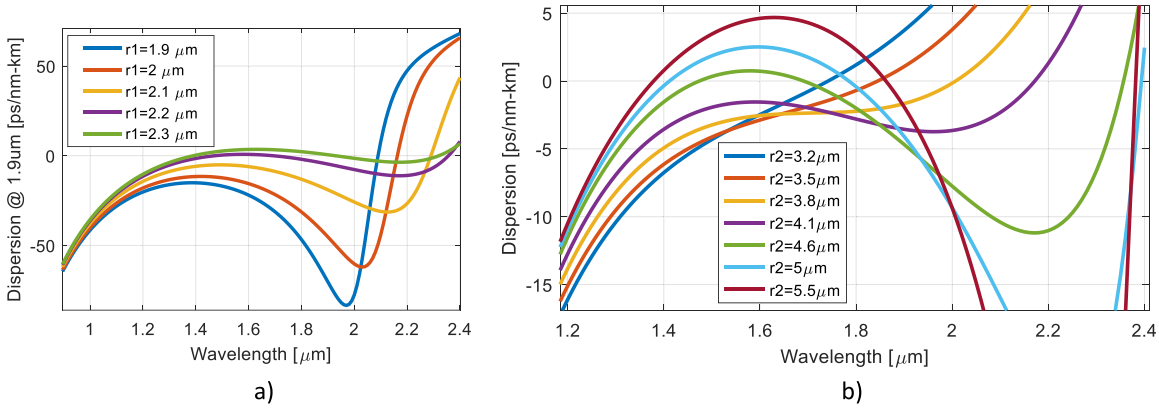

Fig. 4. (a) Plot of dispersion curves as *r1* varies with a fixed $r2 = 4.6$ μm. (b) Plot of dispersion curves as *r2* varies with a fixed $r1 = 2.1$ μm.

overlap with the trench. More interestingly, the increasing core size induces red-shift of the dip, resulting in a broader normal dispersion window to operate in exchange of smaller dispersion value. Overall, a larger core size sees a wider normal dispersion range, better guidance, larger storable energy and a smaller dispersion value. Hence, we can conclude that a smaller core is more suitable to build an oscillator because of its larger normal dispersion value.

While *r1* decreases or *r2* increases, the dispersion curve is developed as a S-shape curve with a hump around 1.6 μm and a dip around 2.2 μm as represented in Fig. 4(b). Consequently, the S curve generates more than one ZDW. With the consideration of a typical Tm operation range of 1.8–2.0 μm, the parametric studies propose acceptable fiber design parameters that satisfy normal dispersion as well as high optical gain in a TDF. For instance, a trench radius of 5.5 μm (the brown curve in Fig. 4(b)) is not acceptable because the cross-over (or ZDW) is located in the middle of the Tm operation region. On the other hand, 5 μm of a trench radius (teal curve) enjoys normal dispersion over the entire Tm band. Likewise, the trench radius of $r2 = 4.6$ μm (green), 4.1μm (purple), and 3.8 μm (yellow) are acceptable. When the radius gets reduces, the normal dispersion turns to anomalous dispersion in the Tm band. With the trench radius of 3.5 μm (the red curve), most of the Tm band experiences anomalous dispersion. And the dispersion becomes entirely anomalous with $r2 = 3.2$ μm (the navy blue curve) at the Tm band.

We summarize the parametric studies in Fig. 5. The furthest ZDW (the ZDW at the longest wavelength) serves well as an indicator to judge if the fiber has normal dispersion in the 2 μm

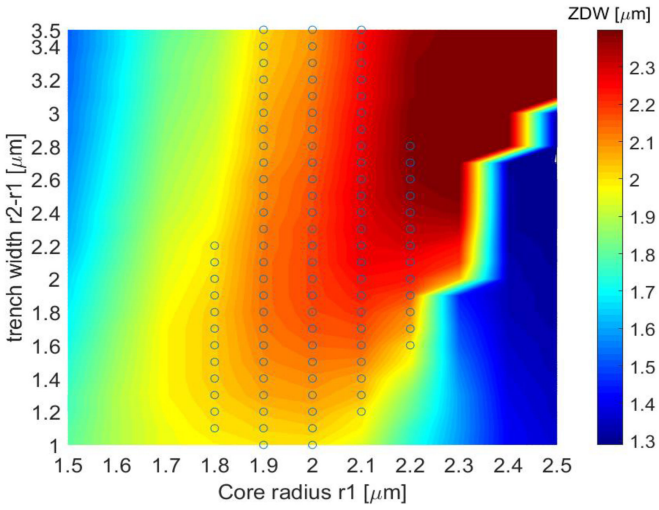

Fig. 5. Contour plot of core size, *r1,* and a trench width, *(r2-r1),* to find furthest ZDW. The circles suggest suitable parameters for normal dispersion operation at the Tm band.

region. Hence, the dispersion behavior is monitored by varying *r1* and (*r2-r1*) to achieve the two required conditions: (i) pushing the furthest ZDW as far into the Infra-Red (IR) range as possible, and (ii) ensuring that the hump does not cause the Tm band to go into anomalous dispersion. This parametric sweep reveals the ranges of acceptable core size and trench size for normal dispersion at the Tm band as the circles marked in Fig. 5.

From Fig. 5, it was concluded that a core radius can vary in the range of 1.8–2.2 μm. As a larger core size is preferred for better guidance and higher storable energy, we select $r1 = 2.2$ μm, $r2 = 4.6$ μm as final design parameters for actual fabrication.

2.2 Fiber Fabrication and Characterization

A TDF with the W-type index profile was fabricated by a conventional MCVD process in conjunction with a solution doping method. A silica soot layer was formed by feeding Oxygen and SiCl4 into a silica substrate tube during the MCVD process. The Tm and Al dopants were introduced to the soot via the solution doping technique. The dopants determine refractive index of the core, Δn_{core}. For the trench region, Fluorine (F) dopant precursor was mixed with $SiCl_4$ to achieve depressed trench index, Δn_{trench}. The fabricated preforms were drawn into two fibers with Outer Diameter (OD) of 130 μm and 145 μm to account for manufacturing tolerance. The fibers will be referred to as A-130 μm and A-145 μm, respectively, in the rest of this paper. An Electron Probe Micro-Analysis (EPMA) was performed on the cross section of the A-130 μm fiber and its results are shown in Fig. 6(a).

The core absorption of A-145 μm fiber was measured using a cut-back method. A supercontinuum source was employed as a light source and transmitted power through a length of A-145 μm fiber was collected on an optical spectrum analyzer (OSA). The obtained absorption spectrum is presented in Fig. 6(b). The peak absorption at 1565 nm is 17.65 dB/m. The A-130 μm fiber has the same absorption rate.

The measured refractive index profiles of the fibers are shown in Fig. 7(a) together with the designed profile. Mainly due to diffusion of dopants, the fabricated fibers exhibit discrepancy from the design in the index profile. To accommodate this fabrication tolerance, we draw a few different fiber diameters. A microscope image of the A-130μm fiber is presented as an inset of Fig. 7(a). We noticed ellipticity in the core.

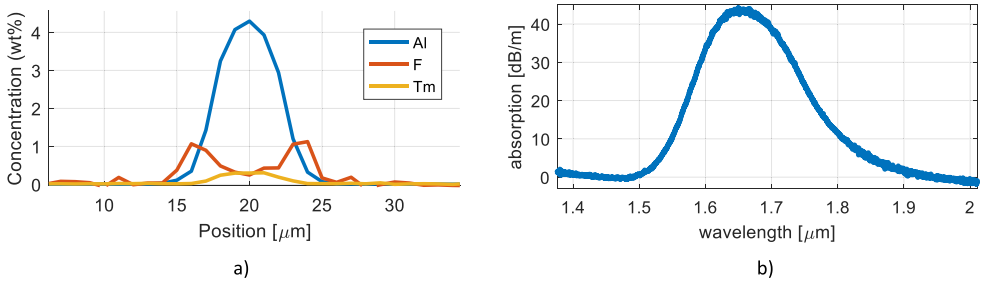

Fig. 6. (a) EPMA results of A-130 μm fiber, showing the doping levels of Al, F, and Tm. (b) Measured absorption curve from A-145 μm.

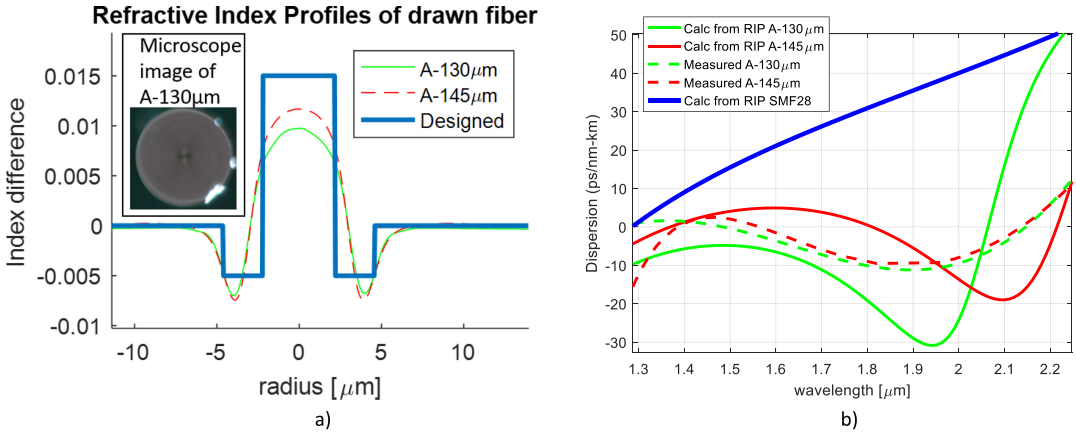

Fig. 7. (a) Measured fiber refractive index profiles (RIPs) of A-130 μm and A-145 μm compared to the design. Inset: Microscope image of A-130 μm fiber. (b) Dispersion curves, both calculated from the RIPs (solid lines) and measured on the interferometer in Fig. 8 (dashed lines) together with dispersion of a standard SMF28.

It is a keen interest to see if the deviation from fabrication tolerance can satisfy the normal dispersion requirement. We used the measured fiber RIPs in Fig. 7(a) to calculate dispersion spectrum in the 2 μm region. Fig. 7(b) shows the calculated dispersion of A-145μm (red solid) and A-130μm (green solid) fibers together with the dispersion curve of the conventional SMF28 (blue) for comparison. The calculated dispersion of SMF28 are ~18.36 ps/nm-km @1550 nm, ~22.01 ps/nm-km @1625 nm and ~35.49 ps/nm-km @1900 nm, which are well matched to measured values of 17 ps/nm-km @1550 nm [29], 21.27 ps/nm-km @1625 nm [29] and 35 ps/nm-km @1900 nm [30], hence validating our calculation. We conclude that the W-type fibers, even with the deviation, see normal dispersion at the 2 μm region thanks to the strong waveguide dispersion. In particular, the A-130 μm fiber shifts the ZDW to beyond 2 μm, resulting in normal dispersion in the range of 1800–2000 nm. As compared to A-140 μm fiber, the smaller core induces stronger waveguide dispersion and dispersion value.

We measured the dispersion of the A-145μm and A-130 μm fibers using an interferometric phase method as described in [29], [31], [32]. A Mach–Zehnder interferometer was set up as shown in Fig. 8(a). The length of fiber under test was ~25 cm and was placed in the test arm. An interferometric fringe spectrum is recorded by an OSA, with a typical fringe as represented in Fig. 8(b).

The fringes are unwrapped using the algorithm described in [29] to obtain the phase $\varphi(\lambda)$ as shown in Fig. 8(b). With the phase, $\varphi(\lambda)$, the group delay, *GD(λ)*, group velocity dispersion parameter, β_2

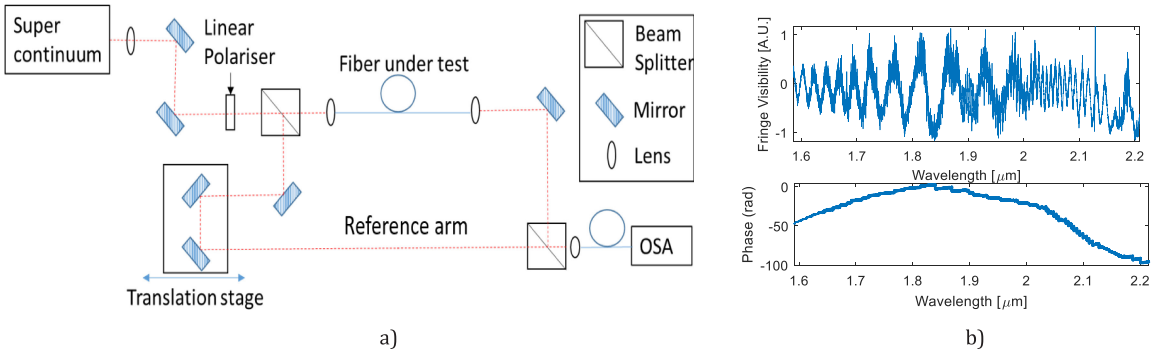

Fig. 8. (a) Experimental setup for dispersion measurement. (b) Top: Interference fringes measured on an OSA. Bottom: Retrieved unwrapped phase, $\varphi(\lambda)$, from the fringes.

(λ), and subsequently dispersion, *D(λ)*, can be obtained by:

$$\varphi(\lambda) = \frac{2\pi}{\lambda}\Delta d \tag{1}$$

$$GD(\lambda) = -\frac{\lambda^2}{2\pi c}\frac{d\varphi(\lambda)}{d\lambda} \tag{2}$$

$$\beta_2(\lambda) = -\frac{\lambda^2}{c}\frac{d^2 n(\lambda)}{d\lambda^2} \tag{3}$$

$$D(\lambda) = -\frac{2\pi c}{\lambda^2}\beta_2(\lambda) \tag{4}$$

where c is speed of light, λ is wavelength, $n(\lambda) = \frac{L_{air}}{L_{air}} \pm \frac{\lambda_\varphi(\lambda)}{2\pi L_{fib}}$ is the effective refractive index, $\Delta d = |L_{air} - n(\lambda)L_{fib}|$ is optical path difference, L_{air} is the optical path length in the reference arm, L_{fib} is the optical path length of fiber arm.

The measured dispersions from the interferometer are shown in Fig. 7(b) with dashed lines. As expected from the calculations based on the fiber RIPs, the two Tm-doped W-type fibers consistently exhibit normal dispersion at the Tm emission band. Considering the ellipticity in index profiles of fabricated fibers (as indicated in the inset of Fig. 7(a)), the measured results are in reasonable agreement with the calculated results. With this, we decide to use the A-130 μm fiber as our Normal Dispersion Tm Fiber (NDTF) to build a cavity because of its slightly larger normal dispersion value.

3. Deployment in Ring Cavity Seed Oscillator

A ring fiber laser oscillator of two different configurations is built to test dispersion dependent laser operation at mode-locking regime. A ring cavity design was chosen as it is simple to implement for all-fiber configuration. The A-130 μm fiber was selected as an active fiber in the oscillators. It is worth to mention here the mode-locking techniques for ultrafast fiber lasers. Using a Saturable Absorber (SA) is a popular technique for building mode-locked lasers. There are a number of technical advances of SA materials capable of creating high energy pulses [33]–[36]. Another widely used method is Nonlinear Polarization Rotation (NPR) technique, where an artificial SA effect is created by nonlinear polarization in the cavity. Since NPR utilizes intensity-dependent change in polarization state and does not depend on any physical SA material, the NPR technique can also be utilized to high energy mode-locking applications.

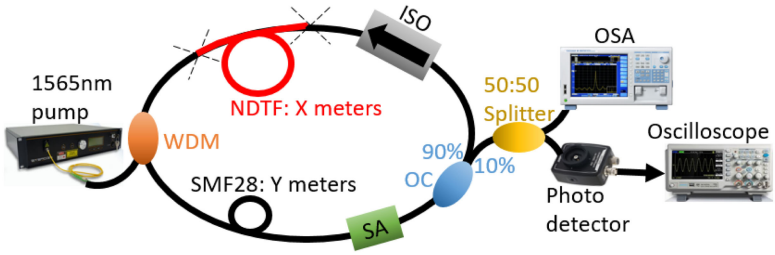

Fig. 9. An experimental setup for both the net anomalous dispersion cavity and also the net close-to-zero-dispersion cavity. For net anomalous cavity, the normal dispersion Tm fiber (NDTF) is ~2.1 m long, and the SMF28 is ~9.9 m long. For net close-to-zero-dispersion cavity, the NDTF is ~2.6 m long, and the SMF28 length is reduced to ~2.1 m. SA: Saturable Absorber, WDM: Wavelength Division Multiplexer, OC: Output Coupler, ISO: Isolator, OSA: Optical Spectrum Analyzer.

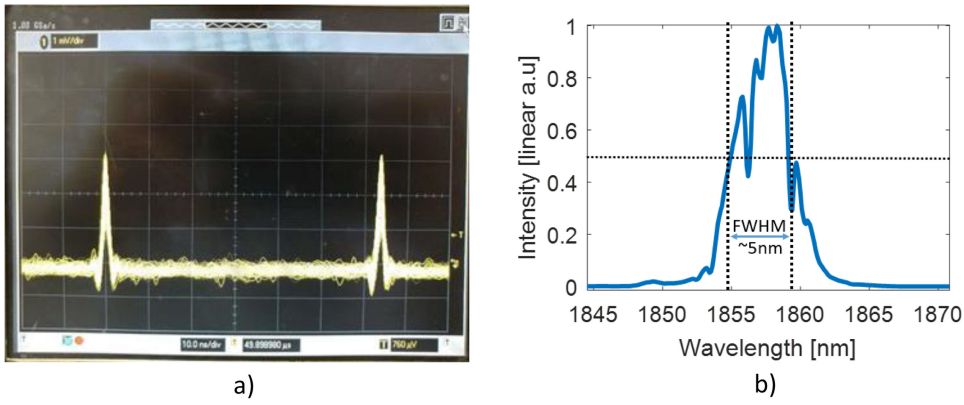

Fig. 10. (a) Measured pulse trace on the oscilloscope and (b) Measured output spectrum on the OSA.

3.1 Net Anomalous Dispersion

First, a ring cavity with net anomalous dispersion was constructed. A schematic of the setup is shown in Fig. 9. The NDTF has normal dispersion while all the passive fibers including the SMF28 and pigtail fibers have anomalous dispersion.

A 1565 nm single mode laser is used as a pump source for core pumping. It can provide up to 2 W pump light. The pump source is coupled into the cavity via a wavelength division multiplexer (WDM). The isolator ensures unidirectional propagation of a signal beam in the anti-clockwise direction. We employed a GaAs based SA with 15% modulation depth at 2 μm for mode-locking. A signal is coupled out through the output coupler with a 10% coupling ratio and its pulse characteristic is diagnosed with the oscilloscope. The cavity contains ~9.9 m of SMF28 and ~2.1 m of NDTF. Subsequently, the total cavity dispersion was estimated as 0.296 ps/nm which is net anomalous dispersion. Because of mismatched mode areas between the NDTF and the SMF28, we had to optimize splicing parameters to reduce the splicing loss. Due to the W-type structure, the conventional method of expanding core size by applying arcs was not helpful to splice the dissimilar fibers. Nonetheless, we managed to reduce the splicing loss to a typical value of ~0.8 dB at each splicing point. Despite a bit higher cavity loss including the splicing loss, the cavity is successfully mode-locked as shown in the oscilloscope trace given in Fig. 10(a).

The mode-locked pulses were characterized with a 2 μm photodetector connected to an oscilloscope. The repetition rate was measured to be ~16.13 MHz This matches to a cavity length of ~12 m. At 35 dBm of pump power, the average output power was measured to be 37 mW. This corresponds to ~0.6 nJ of pulse energy. The spectrum measured on OSA is shown in Fig. 10(b). It has a 3 dB bandwidth of ~5 nm.

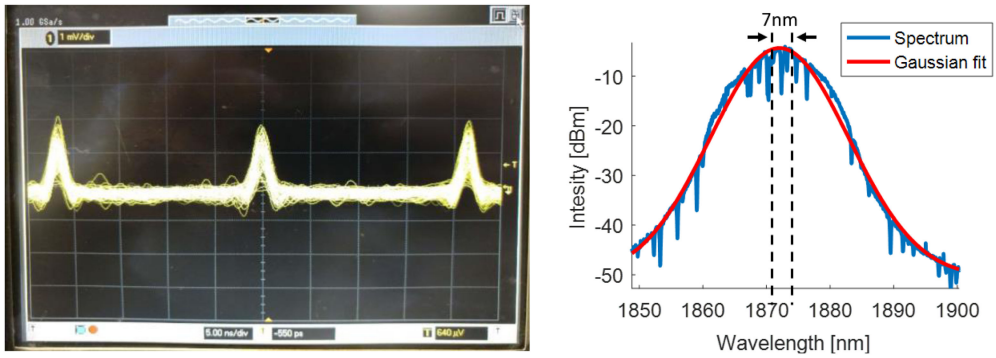

Fig. 11. (a) Measured pulse trace on the oscilloscope and (b) Measured output spectrum on the OSA.

3.2 Net Close-To-Zero Dispersion

In another configuration, the net cavity dispersion was designed to be close to zero. In a net close-to-zero dispersion cavity, the pulse is in the stretched mode and the corresponding pulse spectrum displays a more Gaussian shape with a broad bandwidth. We used the same configuration as in Fig. 9 except the lengths of the fibers are changed for net dispersion control. The length of SMF 28 is reduced to ~2.1 m and the length of NDTF increases to ~2.6 m, which leads to total cavity dispersion of 0.003 ps/nm. Lasing is successful with mode-locking as shown in an oscilloscope trace given in Fig. 11(a).

The measured repetition rate was ~44 MHz which again matches to a cavity length of ~4.7 m. At 32 dBm of pump power, the average output power was measured to be 45 mW. Hence, the calculated pulse energy is 1.02 nJ. The output spectrum is Gaussian-like as expected in the close to zero dispersion cavity. Fig. 11(b) shows the spectrum with a 3-dB bandwidth of ~7 nm. Therefore, we conclude that the fiber indeed offer normal dispersion in the operating wavelength.

4. Deployment of NDTF in All-Fiber Amplifier

We construct all-fiber amplifier using the NDTF. We describe a cavity that generates soliton pulses, and amplifier for pulse energy scaling of the soliton pulses in a normal dispersion regime.

4.1 All-Fiber Seed Oscillator

To generate stable pulses, a ring cavity (seed) laser based on nonlinear polarization rotation (NPR) technique, which is different from the oscillators in Section 3, was employed as illustrated in Fig. 12(a). The pump block consists of External Cavity Laser (ECL) and Erbium amplifier (Er Amp), offering maximum of 2 W of pump power at 1565 nm. The pump beam is coupled into the cavity by the WDM, providing optical pumping to the 1.5 m NDTF. The Polarization Dependent Isolator (PD ISO) ensures unidirectional propagation in the anti-clockwise direction. Mode-locking was achieved through the NPR technique by adjusting Polarization Controllers 1 and 2 (PC1 and PC2). To achieve stable soliton pulses, the oscillator included 55 m of SMF28. The long cavity helps increase non-linearity and reduce pulse repetition rate for higher energy scaling. The generated pulses are out coupled through the 10:90 output coupler, which serves as a seed source to the amplifier stage.

We first characterized the seed pulses before being amplified. The seed output average power was measured at 1 mW. The seed output spectrum shows typical Kelly sidebands indicating soliton operation, shown as the blue curve in Fig. 13(a). The 3 dB bandwidth of the seed spectrum is ~3 nm, which corresponds to ~1.2 ps pulse width assuming a sech^2 -shaped pulse. An InGaAs photodetector was used to measure the pulse repetition rate of ~3 MHz on the oscilloscope, which

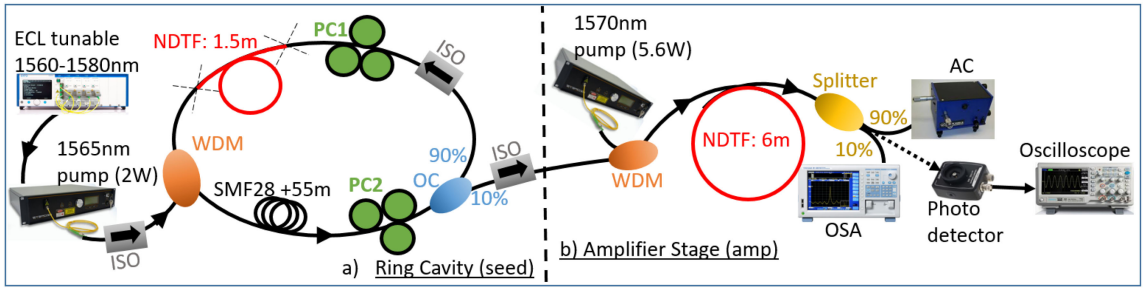

Fig. 12. (a) Schematic of the ring cavity seed laser at near-2μm wavelength region. (b) The output from the seed laser goes into the Amplifier stage, schematic shown. NDTF: Normal Dispersion Tm Fiber; ECL: External Cavity Laser; Er Amp: Erbium Amplifier; WDM: Wavelength Division Multiplexer; PC1 / PC2: Polarization Controller; SMF: Single Mode Fiber; PD: Polarization Dependent; ISO: Isolator; AC: Autocorrelator; OSA: Optical Spectrum Analyzer.

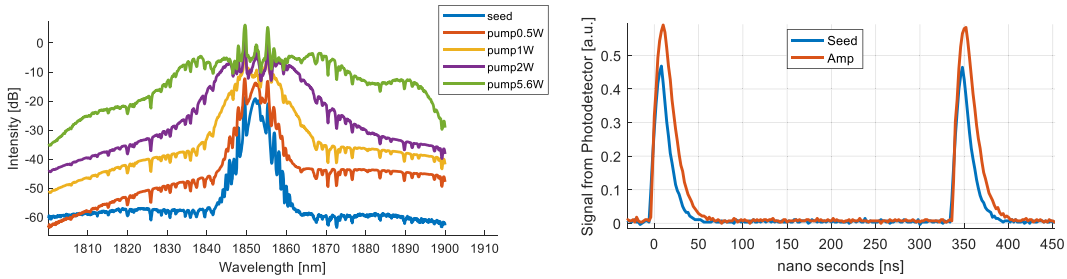

Fig. 13. (a) Spectra of the seed output (blue), and amp output (red, yellow, purple and green) as pump power increases from an OSA. (b) The oscilloscope trace showing output pulses from the seed (blue), and from the amp (red) at full power.

corresponds to the cavity length of ~70 m. The oscilloscope trace is shown as the blue curve on Fig. 13(b). The calculated pulse energy of the seed pulse is ~0.333 nJ, and corresponding calculated peak power is ~277 W.

The amplifier (amp) stage setup is shown in Fig. 12(b). The solitons from the seed oscillator and the 1570 nm pump laser are both coupled into the ~6 m of NDTF through the WDM. As the 1570 nm pump power is increased from 0.5 W up to 5.6 W, the amp output spectrum evolution is observed to have nearly symmetric spectral broadening on the OSA, shown in Fig. 13(a). In addition, using the InGaAs photodetector, the oscilloscope trace of the amp output shows an increase of amplitude without change of the repetition rate as presented with the red curve in Fig. 13(b). Thus, we conclude that the pulse was amplified without breaking-up thanks to the normal dispersion operation. Furthermore, the output power linearly increases with pump power with efficiency of 31.65% as shown in Fig. 14(a). Fig. 14(b) shows an autocorrelator (AC) trace of the amplified pulse at the maximum power.

No indication of pulse breaking is observed on the AC trace. The Full Width Half Max (FWHM) pulse width on the AC trace was measured to be ~2.8 ps. Assuming a Gaussian pulse shape, the pulse width is ~1.98 ps. At the full 5.6 W of pump power to the amp, nearly all pump power was absorbed and the average output power from the amp was 1.66 W. At the maximum power, amplified spontaneous emission (ASE) contribution to the power is estimated about 5% of the total output power, based on OSA spectra. Hence, the obtained pulse energy reaches to ~525 nJ. This is an order of magnitude larger than the prior report from all-fiber configurations [10]. Its corresponding peak power is as high as 188 kW, with >27 dB gain from the seed peak power.

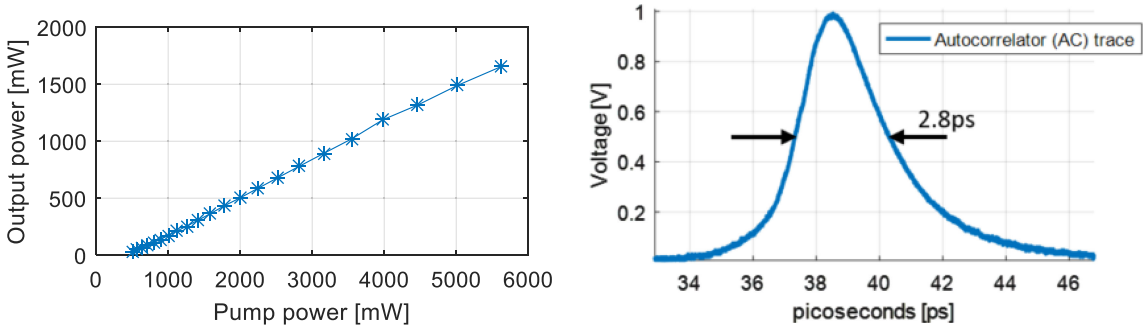

Fig. 14. (a) The output power from the amplifier vs pump power. (b) Autocorrelator (AC) trace showing 2.8 ps FWHM pulse width.

5. Summary and Conclusion

In mode-locked fiber lasers, operating in a normal dispersion regime is a key for pulse energy scaling. However, this requirement has been left unsatisfied at 2 μm, seriously hindering the progress of high pulse energy mode-locked fiber laser at this wavelength region. We reported a normal dispersion Tm doped fiber as a possible solution to this persisting problem. The Tm fiber is designed with a W-type index profile that can adjust dispersion characteristics by introducing strong waveguide dispersion. We provide parametric studies to guide a design. The developed normal dispersion Tm fiber served as a gain medium for both oscillator and amplifier. Mode-locked soliton pulses near 2 μm was amplified to record high pulse energy for an all-fiber setup with pulse energy of $\sim$525 nJ in $\sim$1.98 ps pulse without pulse breaking. This represents high potential for mode-locked pulse energy scaling at 2 μm wavelength in all-fiber configurations.

References

[1] N. Gehlich *et al.*, "Utilizing the transparency of semiconductors via "backside" machining with a nanosecond 2 μm Tm: Fiber laser," *Proc. SPIE*, vol. 8968, 2014, Art. no. 89680W.
[2] IPG Photonics, "Application note #14: Welding clear-to-clear polymers with Thulium fiber lasers," 2014. [Online]. Available: www.ipgphotonics.com
[3] K. Scholle, S. Lamrini, P. Koopmann, and P. Fuhrberg, "2 μm laser sources and their possible applications," *Frontiers in Guided Wave Optics and Optoelectronics*, B. Pal, Ed. Rijeka, Croatia: Intech, 2010.
[4] X. Liu, D. Du, and G. Mourou, "Laser ablation and micromachining with ultrashort pulses," *IEEE J. Quantum Electron.*, vol. 33, no. 10, pp. 1706–1716, Oct. 1997.
[5] A. Hasegawa and M. Matsumoto, *Optical Solitons in Fibers*. New York, NY, USA: Springer, 2002.
[6] Y. Nomura and T. Fuji, "Efficient chirped-pulse amplification based on thulium-doped ZBLAN fibers," *Appl. Phys. Exp.*, vol. 10, 2017, Art. no. 012703.
[7] C. Gaida, M. Gebhardt, T. Heuermann, F. Stutzki, C. Jauregui, and J. Limpert, "Ultrafast thulium fiber laser system emitting more than 1 kW of average power," *Opt. Lett.*, vol. 43, pp. 5853–5856, 2018.
[8] F. Tan, H. Shi, R. Sun, P. Wang, and P. Wang, "1 μJ, sub-300 fs pulse generation from a compact thulium-doped chirped pulse amplifier seeded by Raman shifted erbium-doped fiber laser," *Opt. Exp.*, vol. 24, pp. 22461–22468, 2016.
[9] C. Gaida, M. Gebhardt, F. Stutzki, C. Jauregui, J. Limpert, and A. Tünnermann, "Thulium-doped fiber chirped-pulse amplification system with 2 GW of peak power," *Opt. Lett.*, vol. 41, pp. 4130–4133, 2016.
[10] C. W. Rudy, K. E. Urbanek, M. J. F. Digonnet, and R. L. Byer, "Amplified 2-μm thulium-doped all-fiber mode-locked figure-eight laser," *J. Lightw. Technol.*, vol. 31, pp. 1809–1812, Jun. 2013.
[11] W. H. Renninger, A. Chong, and F. W. Wise, "Pulse shaping and evolution in normal-dispersion mode-locked fiber lasers," *IEEE J. Sel. Topics Quantum Electron.*, vol. 18, no. 1, pp. 389–398, Jan./Feb. 2012.
[12] Y. Tang, A. Chong, and F. W. Wise, "Generation of 8 nJ pulses from a normal-dispersion thulium fiber laser," *Opt. Lett.*, vol. 40, pp. 2361–2364, 2015.
[13] C. W. Rudy, M. J. F. Digonnet, and R. L. Byera, "Advances in 2-μm Tm-doped mode-locked fiber lasers," *Opt. Fiber Technol.*, vol. 20, no. 6, pp. 642–649, 2014.
[14] R. I. Woodward, "Dispersion engineering of modelocked fiber laser," *J. Opt.*, vol. 20, 2018, Art. no. 033002.
[15] F. Haxsen, D. Wandt, U. Morgner, J. Neumann, and D. Kracht, "Pulse energy of 151 nJ from ultrafast thulium-doped chirped-pulse fiber amplifier," *Opt. Lett.*, vol. 35, pp. 2991–2993, 2010.

[16] P. Wan, L.-M. Yang, and J. Liu, "High power 2 μm femtosecond fiber laser," *Opt. Exp.*, vol. 21, pp. 21374–21379, 2013.
[17] R. Andrew Sims, P. Kadwani, A. S. L. Shah, and M. Richardson, "1 μJ, sub-500 fs chirped pulse amplification in a Tm-doped fiber system," *Opt. Lett.*, vol. 38, pp. 121–123, 2013.
[18] F. Stutzki *et al.*, "152 W average power Tm-doped fiber CPA system," *Opt. Lett.*, vol. 39, pp. 4671–4674, 2014.
[19] H. Hoogland and R. Holzwarth, "Compact polarization-maintaining 2.05-μm fiber laser at 1-MHz and 1-MW peak power," *Opt. Lett.*, vol. 40, pp. 3520–3523, 2015.
[20] D. Klimentov, V. V. Dvoyrin, and I. T. Sorokina, "Mode-locked thulium-doped fiber lasers based on normal dispersion active fiber," *IEEE Photon. Technol. Lett.*, vol. 27 no. 15, pp. 1609–1612, Aug. 2015.
[21] C. Gaida, M. Gebhardt, F. Stutzki, C. Jauregui, J. Limpert, and A. Tünnermann, "Thulium-doped fiber chirped-pulse amplification system with 2 GW of peak power," *Opt. Lett.*, vol. 41, pp. 4130–4133, 2016.
[22] F. Tan, H. Shi, P. Wang, J. Liu, and P. Wang, "Chirped pulse amplification of a dissipative soliton thulium-doped fiber laser," *Proc. SPIE*, vol. 9728, 2016, Art. no. 97280Y.
[23] L. Gruner-Nielsen *et al.*, "Dispersion-compensating fibers," *Opt. Fiber. Technol*, vol. 6, no. 2, pp. 164–180, 2000.
[24] P. J. Roberts *et al.*, "Control of dispersion in photonic crystal fibers," in *Fiber Based Dispersion Compensation Optical and Fiber Communications Reports*, vol 5. Berlin, Germany: Springer, 2007.
[25] S. D. Jackson and S. Mossman, "Efficiency dependence on the Tm3+ and Al3+ concentrations for Tm3+-doped silica double-clad fiber lasers," *Appl. Opt.*, vol. 42, pp. 2702–2707, 2003.
[26] R. Sidharthan *et al.*, "Step-index high-absorption Yb-doped large-mode-area fiber with Ge-doped raised cladding," *Opt. Lett.*, vol. 43, pp. 5897–5900, 2018.
[27] G. P. Agrawal, *Nonlinear Fiber Optics*, 4th ed. New York, NY, USA: Academic Press, 2006.
[28] S. Ramachandran, *Fiber Based Dispersion Compensation*. Berlin, Germany: Springer, 2007.
[29] W. Qi, X. Huang, D. Ho, S. Yoo, K. T. Yong, and F. Luan, "Dispersion measurement of optical fibers by phase retrieval from spectral interferometry," *J. Opt.*, vol. 19, no. 5, 2017, Art. no. 055611.
[30] Q. Q. Wang, T. Chen, M. Li, B. Zhang, Y. Lu, and K. P. Chen, "All-fiber ultrafast thulium-doped fiber ring laser with dissipative soliton and noise-like output in normal dispersion by single-wall carbon nanotubes," *Appl. Phys. Lett.*, vol. 103, 2013, Art. no. 011103.
[31] P. Hlubina, M. Kadulová, and D. Ciprian, "Spectral interferometry-based chromatic dispersion measurement of fibre including the zero-dispersion wavelength," *J. Eur. Opt. Soc. Rapid Publications*, vol. 7, 2012, Art. no. 12017.
[32] S. Rao D. S. *et al.*, "Ultra-low-noise supercontinuum generation with a flat near-zero normal dispersion fiber," *Opt. Lett.*, vol. 44, pp. 2216–2219, 2019.
[33] B. Guo *et al.*, "Sub-200 fs soliton mode-locked fiber laser based on bismuthene saturable absorber," *Opt. Exp.*, vol. 26, pp. 22750–22760, 2018.
[34] J. He, L. Tao, H. Zhang, B. Zhouc, and J. Lia, "Emerging 2D materials beyond graphene for ultrashort pulse generation in fiber lasers," *Nanoscale*, vol. 11, pp. 2577–2593, 2019.
[35] Y. Ge *et al.*, "Broadband nonlinear photoresponse of 2D TiS_2 for ultrashort pulse generation and all-optical thresholding devices," *Adv. Opt. Mater.*, vol. 6, no. 4, 2018, Art. no. 201701166.
[36] P. Li *et al.*, "Two-dimensional CH3NH3PbI3 perovskite nanosheets for ultrafast pulsed fiber lasers," *ACS Appl. Mater. Interfaces*, vol. 9, pp. 12759–12765, 2017.